Prolonged seizure activity impairs mitochondrial bioenergetics and induces cell death

Stjepana Kovac[1,2], Ana-Marija Domijan[3], Matthew C. Walker[1] and Andrey Y. Abramov[1,*]

[1]UCL Institute of Neurology, University College London, Queen Square, London WC1N 3BG, UK
[2]Department of Neurology, University of Muenster, 48129 Muenster, Germany
[3]Unit of Toxicology, Institute for Medical Research and Occupational Health, 10001 Zagreb, Croatia
*Author for correspondence (a.abramov@ucl.ac.uk)

Accepted 20 November 2011
Journal of Cell Science 125, 1796–1806

doi: 10.1242/jcs.099176

Summary

The mechanisms underlying neuronal death following excessive activity such as occurs during prolonged seizures are unclear, but mitochondrial dysfunction has been hypothesised to play a role. Here, we tested this with fluorescence imaging techniques in rat glio-neuronal neocortical co-cultures using low Mg^{2+} levels to induce seizure-like activity. Glutamate activation of NMDA receptors resulted in Ca^{2+} oscillations in neurons and a sustained depolarisation of the mitochondrial membrane potential, which was cyclosporine A sensitive, indicating mitochondrial permeability and transition pore opening. It was also dependent on glutamate release and NMDA receptor activation, because depolarisation was not observed after depleting vesicular glutamate with vacuolar-type H^+-ATPase concanamycin A or blocking NMDA receptors with APV. Neuronal ATP levels in soma and dendrites decreased significantly during prolonged seizures and correlated with the frequency of the oscillatory Ca^{2+} signal, indicative of activity-dependent ATP consumption. Blocking mitochondrial complex I, complex V or uncoupling mitochondrial oxidative phosphorylation under low-Mg^{2+} conditions accelerated activity-dependent neuronal ATP consumption. Neuronal death increased after two and 24 hours of low Mg^{2+} levels compared with control treatment, and was reduced by supplementation with the mitochondrial complex I substrate pyruvate. These findings demonstrate a crucial role for mitochondrial dysfunction in seizure-activity-induced neuronal death, and that strategies aimed at redressing this are neuroprotective.

Key words: Cell death, Seizure, Status epilepticus, Mitochondria, ATP, Neurons

Introduction

Cell death in seizures has been observed in in vitro and in vivo models of epilepsy and is the hallmark of hippocampal sclerosis, the commonest pathology associated with epilepsy (Deshpande et al., 2008; Swanson, 1995). This neuronal death is critically dependent upon excessive neuronal activity, as seen in status epilepticus (Pitkänen et al., 2002). Such activity induces large ionic shifts with consequent demands for energy substrates to maintain transmembrane ion homeostasis. Biochemical studies of brain homogenates have revealed decreased ATP concentrations after repeated seizures and seizure-induced energy failure has long been suggested as a reason for clinical sequelae in prolonged seizures (Wasterlain et al., 1993). However, the mechanisms that result in a failure of neurons to compensate during this period of increased energy demand are unclear. ATP production is closely linked to the mitochondrial membrane potential ($\Delta\psi_m$) because the electrochemical proton gradient across the inner mitochondrial membrane is a prerequisite for ATP synthesis (Mitchell and Moyle, 1965). Mitochondrial membrane potential depolarisation reduces the mitochondrial functional capacity for producing ATP and Ca^{2+} buffering, and thus leads to mitochondrial dysfunction in various CNS pathologies (Abramov and Duchen, 2010; Damiano et al., 2010; Distelmaier et al., 2009). But are these changes sufficient to explain the failure of ATP production and the subsequent neuronal death? Studies in which supplementation of animals with mitochondrial substrates reduces neuronal death point to a process of energy and mitochondrial failure as mechanisms underlying seizure-induced neuronal death; however, more direct evidence to support this hypothesis is lacking (Kim et al., 2007; Yi et al., 2007). Moreover, there is growing evidence of an important role for astrocytes in generating and maintaining seizure activity (Gómez-Gonzalo et al., 2010), yet the relative roles of seizure activity on astrocytic and neuronal mitochondrial membrane potential and ATP levels are unknown.

The low-Mg^{2+} culture model of epilepsy has provided a powerful tool to investigate the influence of prolonged seizure activity (Deshpande et al., 2008). Importantly, using this model, we can establish the contribution of pure neuronal activity on ATP depletion without confounding it with effects of cerebral blood flow changes and systemic metabolic changes as seen in in vivo models of convulsive seizures. Estimating the contribution of epileptiform neuronal activity on ATP depletion is important because status epilepticus might present without positive motor symptoms as in non-convulsive status epilepticus. Conceptually, the low-Mg^{2+} model of epilepsy greatly differs from studies on models of direct pharmacological activation of glutamate receptors, insofar as it does not rely on excessive activation by drugs. Moreover, reduced divalent cations and Mg^{2+} have been found during excessive neuronal firing, which is the hallmark of epilepsy, and are well known electrolyte imbalances that lead to seizures in human (Rusakov and Fine, 2003; Castilla-Guerra et al., 2006).

Journal of Cell Science

Using this model, we show here that seizure-induced, NMDA receptor-dependent neuronal Ca^{2+} oscillations correlate with mitochondrial membrane depolarisation and a decrease in ATP levels, leading to cell death. This is the first time that a link between mitochondrial membrane potential depolarisation, ATP depletion and cell death has been shown as a result continuous seizure activity. Moreover, pharmacologically impairing mitochondrial function accelerated ATP consumption, whereas rescuing mitochondrial function by providing the mitochondria substrate pyruvate prevented neuronal death. We thus provide compelling evidence of Ca^{2+}-induced mitochondrial dysfunction as a substrate for seizure-induced neuronal death and suggest that targeting this can be neuroprotective.

Results

Ca^{2+} changes during epileptiform activity

The omission of Mg^{2+} from the solution induced a synchronised Ca^{2+} signal in the neuronal culture (Fig. 1A, $n=182$ neurons). Low- Mg^{2+}-induced Ca^{2+} spikes were observed in $33.5\pm4.7\%$ of neurons. Repetitive Ca^{2+} signals had amplitudes of 0.50 ± 0.02 (min. 0.06 max. 2.47; amplitude of Fura-2 ratio). The delay to the onset of repetitive Ca^{2+} spikes was 2.51 ± 0.16 minutes and the mean frequency was 0.64 ± 0.02 Ca^{2+} spikes per minute ($n=182$). Ca^{2+} signals were in the nanomolar range, as they were observed with Fura-2 but not with the low-affinity Ca^{2+} indicator Fura-FF ($n=29$; data not shown).

The high-frequency oscillatory $[Ca^{2+}]_c$ signal had the appearance of IP3-mediated $[Ca^{2+}]_c$ release from the ER. However, depletion of the internal Ca^{2+} stores by pre-application of the sarco- or endoplasmic reticulum Ca^{2+} ATPase (SERCA) inhibitor thapsigargin (0.5 μM) did not block low-Mg^{2+}-induced Ca^{2+} oscillations ($n=15$), but rather significantly increased the frequency of the signal (0.77 ± 0.03 vs 1.02 ± 0.04, $P<0.001$; Fig. 1B). We could prevent the Ca^{2+} signal by using a Ca^{2+}-free (+EGTA 0.5 mM) low-Mg^{2+} solution ($n=20$), suggesting that the low-Mg^{2+}-induced oscillations are the result of influx of extracellular Ca^{2+}.

L-type Ca^{2+} channel blocker verapamil (20 μM) did not abolish low-Mg^{2+}-induced Ca^{2+} oscillations. It significantly increased the frequency of the Ca^{2+} spikes by ~30% (0.66 ± 0.07 vs 1.0 ± 0.06 spikes per minute; $P<0.001$), but had no effect on the amplitude of the repetitive Ca^{2+} signals ($P>0.05$; $n=38$; Fig. 1C). Removal of Mg^{2+} enhances the excitatory drive in neuronal networks by abolishing the voltage-dependent blockade of NMDA glutamate receptors (Ascher et al., 1988). We found that D-2-amino-5-phosphonovaleric acid (APV; 25 μM) both prevented the occurrence of discharges ($n=16$) and blocked established discharges ($n=30$, Fig. 1D). To test whether activity in the low-Mg^{2+} model of epilepsy is dependent on vesicular glutamate release, we depleted vesicular glutamate from the ready-releasable pool, by incubating the neuronal cultures with the specific inhibitor of the vacuolar-type H^+-ATPase concanamycin A (5 μM; 2 hours) before exposure to low-Mg^{2+} medium. Incubation with concanamycin A prevented the low-Mg^{2+}-induced activity ($n=45$), implying that vesicular glutamate release is an essential mechanism in the low-Mg^{2+} seizure model.

We also observed Ca^{2+} changes in astrocytes. Compared with the high signal observed in neurons, the Ca^{2+} changes measured

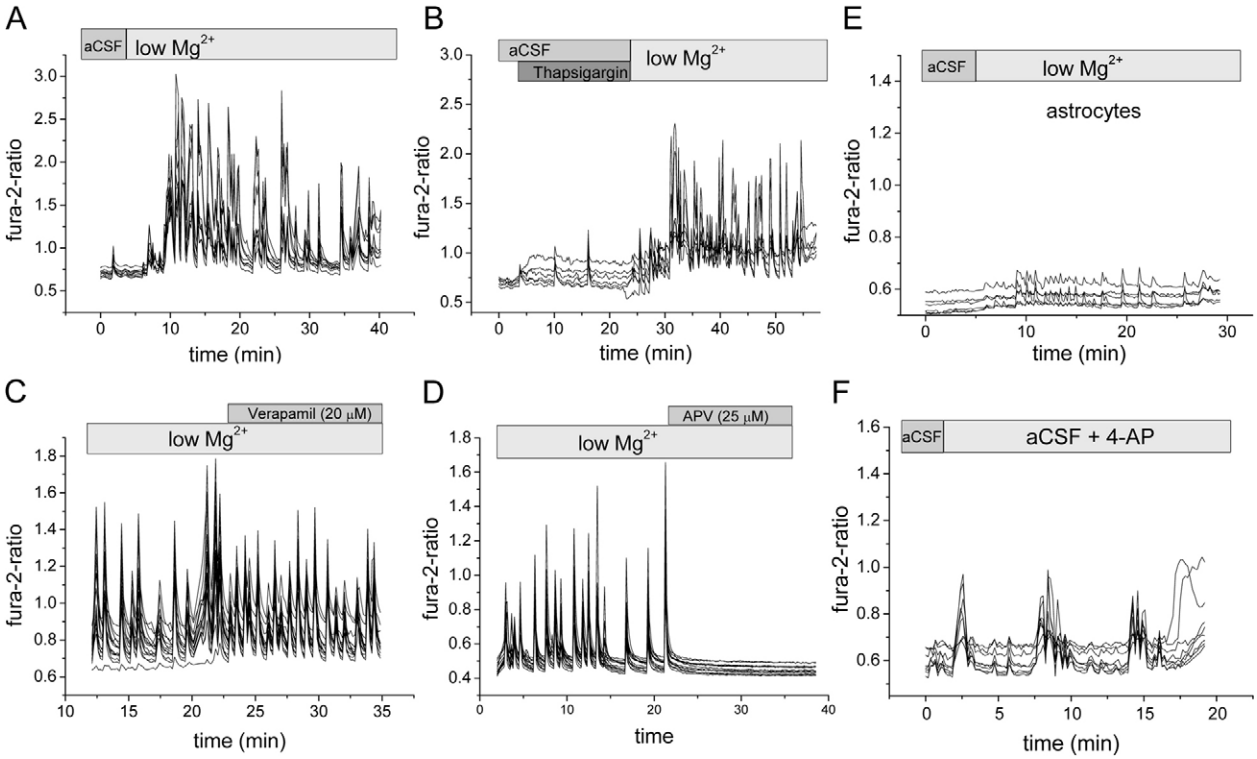

Fig. 1. Characteristics and pharmacology of low-Mg^{2+}-induced Ca^{2+} signals in neurons. Replacement of aCSF with low-Mg^{2+} aCSF induces synchronous oscillatory Ca^{2+} signals (**A**), which are modified but not abolished by SERCA inhibitor thapsigargin (0.5 μM) (**B**). Neuronal Ca^{2+} signals increase in frequency when verapamil (20 μM) is bath applied (**C**) and Ca^{2+} signals are abolished when NMDA receptors are blocked with APV (25 μM) (**D**). (**E**) Ca^{2+} signals were also observed in astrocytes. (**F**) Ca^{2+} signals are reproduced in neurons in the 4-AP epilepsy model.

in astrocytes, using Fura-2 ratio fluorescence, were small in amplitude (Fig. 1E). To confirm that periodic synchronous Ca^{2+} oscillations were not a peculiarity of this model, we tested whether these could be elicited using another in vitro epilepsy model. The well-established convulsant 4-aminopyridine (4-AP) also induced synchronous Ca^{2+} spikes; these were, however, smaller in amplitude and less frequent (Fig. 1F). Because large Ca^{2+} influxes can affect mitochondrial function, we next asked whether the mitochondrial membrane potential, measured with the fluorescent indicator Rhodamine123, was altered by these Ca^{2+} oscillations.

Mitochondrial membrane potential changes

In artificial cerebrospinal fluid (aCSF), small intracellular Ca^{2+} changes did not evoke mitochondrial membrane potential changes. We found that removal of Mg^{2+} induced changes in mitochondrial membrane potential ($\Delta\psi_m$). Mitochondrial membrane potential changes were observed both in the soma and dendrites of the neurons with dendrites showing transient (Fig. 2A,B) and somata sustained mitochondrial membrane depolarisations (Fig. 2C,D). Overall, there was a significant $12\pm0.7\%$ decrease in the mitochondrial membrane potential of neurons that showed repetitive Ca^{2+} oscillations after 5 minutes of low-Mg^{2+} treatment ($P<0.001$) and the $\Delta\psi_m$ further decreased when compared with baseline after 10, 15 and 20 minutes of low-Mg^{2+} treatment (one-way ANOVA; $P<0.001$).

However, depolarisation was not uniform. Whereas some neurons showed large decreases in mitochondrial membrane potential others either did not show or showed only marginal changes in $\Delta\psi_m$. We hypothesised that those neurons with larger depolarisation in $\Delta\psi_m$ experienced a longer and higher exposure to Ca^{2+}.

Simultaneous recording of Ca^{2+} spikes during measurements of mitochondrial membrane potential allowed the correlation of Ca^{2+}, as measured by Fura-2 ratio, to the mitochondrial membrane potential, measured with Rhodamine123. We found a significant inverse correlation of the mitochondrial membrane potential at the 5, 10, 15 and 20 minute time points with the delay in onset of Ca^{2+} spikes ($n=182$; Pearson correlation coefficient, 0.264, $P<0.05$, $P<0.05$, $P<0.01$ and $P<0.05$ for each of the respective time points), suggesting that mitochondrial membrane potential depolarisation is linked to the onset of continuous spiking activity. To focus further on neurons that showed prominent mitochondrial membrane potential changes and thus are more likely to be exposed to high levels of Ca^{2+}, we classified mitochondrial membrane potential change as significant when the fluorescence increase was at least 10% of that elicited by FCCP. With this cut-off, ~50% of the neurons exhibited a change of the mitochondrial membrane potential. Analysis of the time course of the $\Delta\psi_m$ in those neurons revealed that the depolarisation increased significantly within 20 minutes of exposure to the low-Mg^{2+} medium (one-way ANOVA, $P<0.001$; Fig. 3A,B). Post-hoc analysis revealed a significant increase of the mitochondrial membrane potential between 5 minutes and 15 minutes ($P<0.05$) and 5 minutes and 20 minutes ($P<0.001$, Tukey's post-hoc test; Fig. 3B).

We found that the depolarisation of the neuronal $\Delta\psi_m$ was accompanied by a hyperpolarisation of the astrocytic $\Delta\psi_m$ following the onset of Ca^{2+} spiking (Fig. 3C,D). Applying the same criteria of a 10% alteration in fluorescence as a significant hyperpolarisation, we observed a significant hyperpolarisation of astrocytes throughout the 20 minute time window (Fig. 3C,D).

Considering that in previous studies prolonged glutamate exposure induces MPTP opening (Abramov and Duchen, 2008), we tested whether the MPTP blocker cyclosporin A (CsA, 1 μM) affected mitochondrial membrane potential during low-Mg^{2+} exposure. Surprisingly, CsA abolished the early depolarisation in our experiments. The neuronal mitochondrial membrane potential after 5, 10 and 15 minutes of treatment with low-Mg^{2+} solution did not differ from baseline treatment (set as 0, normalised) ($P>0.05$). However, 20 minutes after the low-Mg^{2+} treatment, neuronal mitochondrial depolarisation reached significance ($P<0.01$) when compared with the baseline, suggesting that there is still mitochondrial membrane potential depolarisation that is not linked to MPTP opening (Fig. 3E). It should be noted that this mitochondrial membrane potential depolarisation was not

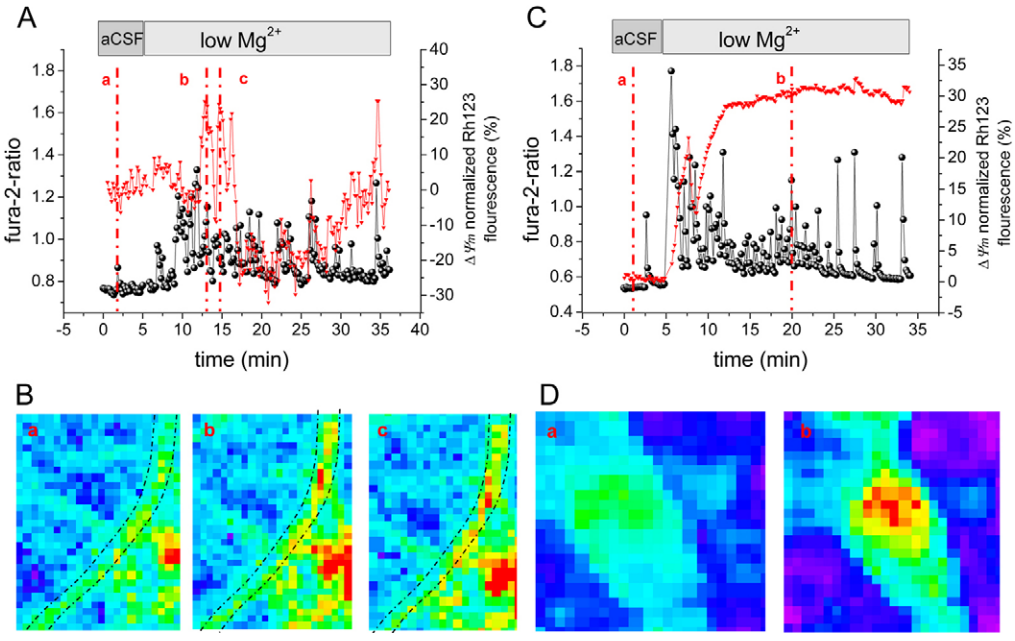

Fig. 2. Low Mg^{2+} induces $\Delta\psi_m$ changes in somata and dendrites of neurons. (**A**,**B**) Low-Mg^{2+}-induced Ca^{2+} signal (black trace) and corresponding mitochondrial membrane potential measured with Rhodamine123 ($\Delta\psi_m$; red trace) in a dendrite. Note that mitochondrial membrane depolarisation is time locked to the dendritic Ca^{2+} rises (A). Colour-coded Rhodamine123 fluorescence of the dendrite at three different time points (a,b,c) as marked in A (B). (**C**) Low-Mg^{2+}-induced Ca^{2+} signal (black trace) and corresponding mitochondrial membrane potential measured with Rhodamine123 ($\Delta\psi_m$; red trace) in the soma of a neuron. (**D**) Colour-coded Rhodamine123 fluorescence of the soma at two different time points (a,b) as marked in C, showing depolarisation of the soma in low-Mg^{2+} conditions.

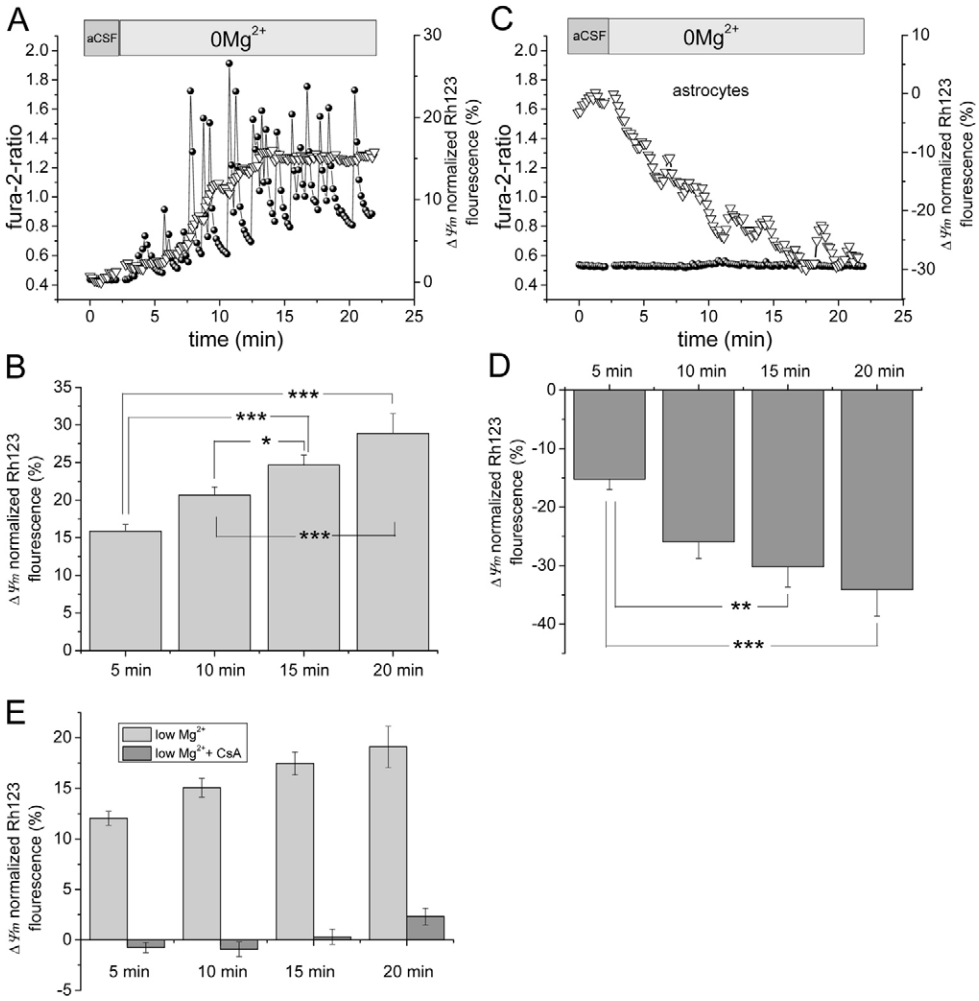

Fig. 3. Inverse relation of low-Mg^{2+}-induced $\Delta\psi_m$ changes of neurons when compared with astrocytes. (**A**) Low-Mg^{2+}-induced Ca^{2+} signal (black dots) and corresponding mitochondrial membrane potential measured with Rhodamine123 ($\Delta\psi_m$; black triangles) in a single neuron. (**B**) Normalised Rhodamine123 fluorescence of neurons that responded to the low-Mg^{2+} treatment at different time points of low-Mg^{2+} exposure. Note that the initial depolarisation is followed by a steady increase of the depolarisation over a time period of 20 minutes. (**C**) A decrease of the mitochondrial membrane potential measured with Rhodamine123 is seen in astrocytes (triangles) and the corresponding Ca^{2+} signal (circles) in a single astrocyte. (**D**) Normalised astrocytic Rhodamine123 fluorescence showing significant steady decreases of the mitochondrial membrane potential within a period of 20 minutes. (**E**) Neuronal mitochondrial membrane potential depolarisation is blocked by cyclosporine A. Results show mean ± s.e.m. *P<0.05; **P<0.01; ***P<0.001.

observed in experiments where the Ca^{2+} influx was blocked with APV (25 μM) and Ca^{2+}-free (+EGTA 0.5 mM) low-Mg^{2+} solution. Mitochondrial membrane potential depolarisation was also abolished after incubation with concanamycin A (5 μM, 2 hours), suggesting that depolarisation was dependent on Ca^{2+} influx through glutamate-induced NMDA receptor activation (n=111).

ATP levels during low-Mg^{2+}-induced activity

The prominent $\Delta\psi_m$ depolarisation, suggests that Mg^{2+}-free medium induces an energy collapse in some cells, leading to Ca^{2+}-induced depolarisation of the mitochondrial membrane potential. To investigate the energetic status of neurons during low-Mg^{2+} treatment, we used the low-affinity Mg^{2+} indicator MAG-Fura for indirect measurements of ATP levels of cells (Abramov and Duchen, 2010). Considering that Ca^{2+} changes were not observed in experiments performed with the low-affinity Ca^{2+} indicator Fura-FF, we suggest that changes in MAG-Fura fluorescence are not related to Ca^{2+} changes. The vast majority of ATP is bound to intracellular Mg^{2+} (Corkey et al., 1986) and therefore, increases in MAG-Fura fluorescence indicate dissociation of Mg^{2+} from ATP and so directly reflect cellular ATP decrease. We found that omission of Mg^{2+} from the medium induced immediate increases in cytosolic Mg^{2+} concentration (Fig. 4A).

We observed two different patterns of Mg^{2+} changes. Stepwise increases of Mg^{2+} were seen in the early phases of Mg^{2+} replacement and were time locked to rises in Ca^{2+} (Fig. 4A). In addition, we observed a continuous increase in Mg^{2+} concentration in neurons (Fig. 4B), which was not observed in astrocytes (Fig. 4C). Analysis of the normalised MAG-Fura ratio in neurons showed that there was a continuous significant increase in Mg^{2+}, reflecting continuous ATP decreases at 10, 20, 30 and 40 minutes when compared with the baseline (one-way ANOVA, P<0.001; Fig. 4D).

We hypothesised that energy deprivation as reflected by rises in Mg^{2+} are linked to the frequency of Ca^{2+} rises. Simultaneous recording of Ca^{2+} (Fluo-4) and Mg^{2+} (Mag-Fura) allowed correlations of these parameters. The frequency of the Ca^{2+} rises correlated significantly with the MAG-Fura ratio at 30 minutes (r=0.513; P<0.01) suggesting that energy deprivation is linked to the oscillatory Ca^{2+} signal (Fig. 4E). Given that Ca^{2+} changes, $\Delta\psi_m$ depolarisation and ATP decreases occur sequentially, we hypothesised that they were inter-related. Therefore we asked whether we could induce rapid energy deprivation by pretreating cells with mitochondrial oxidative phosphorylation uncoupler FCCP (0.5 μM), complex I inhibitor rotenone or complex V inhibitor oligomycin. We found that pretreatment of neurons with FCCP (n=77; 0.5 μM) before replacement with a low-Mg^{2+} solution leads to massive ATP

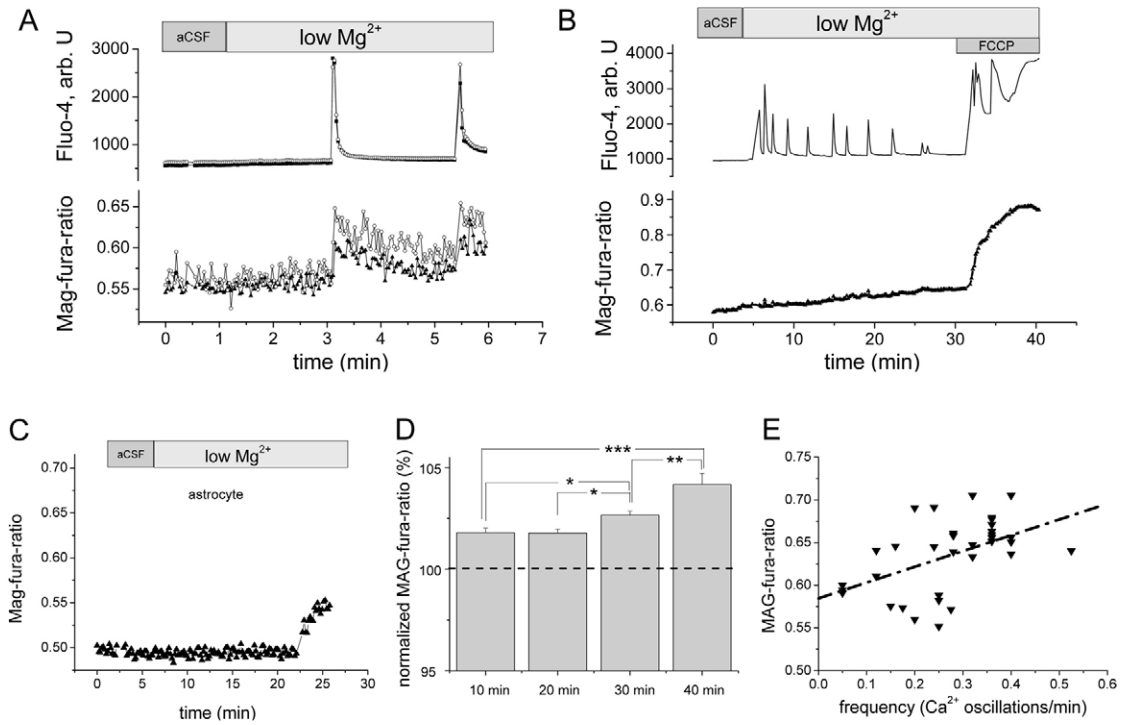

Fig. 4. Low Mg^{2+} induced changes in ATP as measured by MAG-Fura ratios and corresponding Ca^{2+} changes. Change in Fluo-4 fluorescence and changes in corresponding MAG-Fura ratios. Two distinct patterns of changes in MAG-Fura were observed in neurons. (**A**) Step-like increase of the MAG-Fura ratio (bottom panel) time locked to the Ca^{2+} rises measured by Fluo-4 (top panel) in two neurons. (**B**) Steady-state increase of MAG-Fura ratio (bottom panel) in a neuron that shows repetitive Ca^{2+} signal (top panel). Note the different time resolutions in A and B. (**C**) MAG-Fura ratios remain unchanged in astrocytes. Trace shows MAG-Fura ratio in a single astrocyte. (**D**) Normalised MAG-Fura ratios in neurons are significantly higher at 10, 20, 30 and 40 minutes of treatment when compared with baseline (aCSF; dotted line). Results show mean ± s.e.m. *P<0.05; **P<0.01; ***P<0.005. (**E**) Neuronal intracellular Mg^{2+} concentration at a late time point correlates with the frequency of the oscillatory Ca^{2+} signal.

depletion. This energetic collapse was induced by the first Ca^{2+} oscillations, suggesting an activity-dependent mechanism (Fig. 5A). Astrocytes showed a Ca^{2+} peak when pretreated with FCCP in aCSF. In contrast to neurons, astrocytes (n=21) lacked the low-Mg^{2+}-induced Ca^{2+} changes and showed only moderate increases in Mg^{2+} (Fig. 5B). To strengthen the hypothesis that neuronal mitochondrial membrane potential depolarisation, PTP opening and ATP decreases are interrelated we pretreated cells with FCCP (0.5 μM) and CsA (1 μM). CsA pretreatment delayed the FCCP-induced ATP depletion under low-Mg^{2+} conditions (P<0.001) and reduced the maximal cytosolic Ca^{2+} signal when compared with that in cells pretreated with FCCP alone (n=38; P<0.001, Fig. 5C,D). FCCP produced complete $\Delta\psi_m$ depolarisation, which can block mitochondrial Ca^{2+} uptake and change cytosolic Ca^{2+} signal. To avoid misinterpretation of the results, we used oligomycin, which inhibits ATP production but does not decrease $\Delta\psi_m$, or an inhibitor of mitochondrial respiration rotenone. Rapid ATP depletion was induced by both complex I inhibition with rotenone (1 μM; n=36) and complex V (ATP synthetase) inhibition with oligomycin (0.2 μg/ml; n=22; Fig. 7A–C). It should be noted that in some experiments, application of rotenone inhibited Ca^{2+} oscillations.

To verify that the changes in ATP observed were definitely due to ATP decreases, we measured ATP levels inside neurons and astrocytes using a genetically encoded fluorescent ATP indicator (AT1.03 or mitAT1.03) in a subset of cells (generously provided by Hiromi Imamura (The Hakubi Center & Graduate School of Biostudies, Kyoto University) (Imamura et al., 2009). Moreover, in these experiments, we aimed to investigate whether there were differences in ATP levels and changes in the soma when compared with the dendrites. ATP decreases were observed in neurons after low-Mg^{2+} exposure with both AT1.03 and mitAT1.03 fluorescent indicators (n=6; Fig. 6A–C). Baseline levels of ATP differed depending on the region of interest, with higher ATP levels in the soma when compared with the dendrites of neurons (Fig. 6B). However, the time course of ATP depletion did not differ between the two regions. When compared with neurons, astrocytes showed no decrease or only very small decreases in ATP levels during epileptiform activity (n=5; Fig. 6D,E,H). Pretreatment with rotenone (5 μM) and oligomycin (0.2 μg/ml) had no impact on astrocytic ATP levels during epileptiform activity, whereas inhibition of glycolysis with IAA (100 μM) induced rapid ATP depletion during low-Mg^{2+} conditions (n=4; Fig. 6E). Mitochondrial uncoupling with FCCP (0.5 μM) accelerated ATP depletion in both neurons (n=4) and astrocytes (n=5), suggesting a high impact of glycolysis in astrocytes (Fig. 6F,G).

Cell-death analysis

We further hypothesised that ATP depletion in conditions of low Mg^{2+} can induce cell death after a long exposure. There was no significant difference in the neuronal death 10 minutes after treatment with either aCSF (n=15; 14.7±2.4%) or low Mg^{2+} (n=15; 17.2±2.8%; P>0.05). However, there was a significant

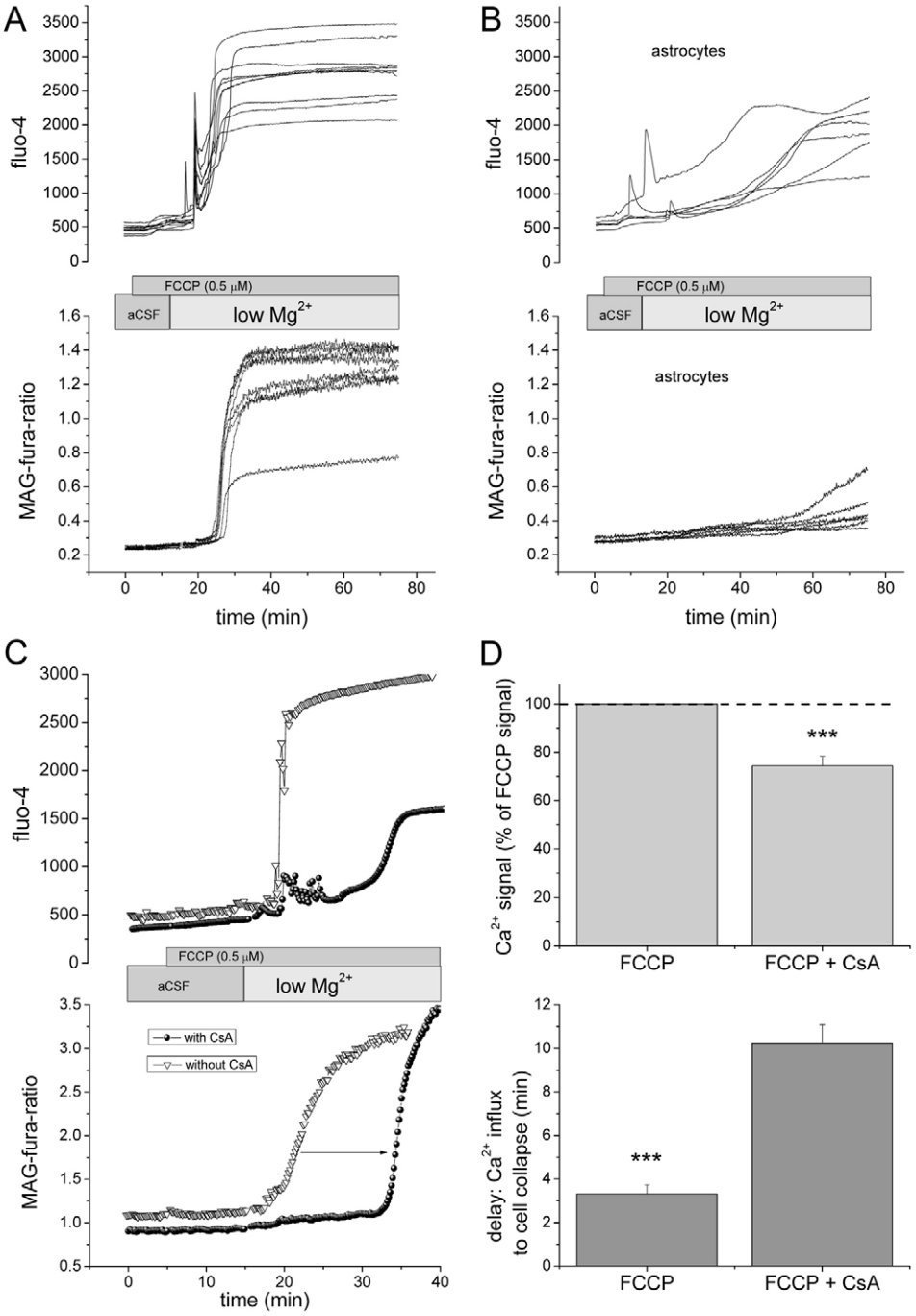

Fig. 5. ATP depletion and mitochondrial uncoupling. Low-Mg^{2+}-induced ATP depletion is accelerated in neurons (**A**) and to a lesser extent in astrocytes (**B**) after pretreatment with mitochondrial uncoupler FCCP (0.5 μM). After initial oscillatory Ca^{2+} signal induced by low-Mg^{2+} conditions neurons exhibit an excessive intracellular Ca^{2+} rise measured by Fluo-4 (top panel). These changes induce excessive MAG-Fura ratio increase (bottom panel; A). In astrocytes single Ca^{2+} signals are observed during pretreatment with FCCP (0.5 μM). Note that, in contrast to neurons in astrocytes, these peaks coincide with the initial application of FCCP in aCSF and are not seen in low-Mg^{2+} condition (top panel). MAG-Fura ratios are only moderately increased in astrocytes compared with neurons (bottom panel; B). (**C**,**D**) Rapid ATP depletion is delayed after pretreating neurons with CsA. FCCP-induced cell collapse and maximum cytosolic Ca^{2+} load is reduced when CsA is added to the FCCP-treated neurons. Results show mean ± s.e.m. ***$P<0.001$.

difference in neuronal death after 2 hours between the two treatment groups. Cultures exposed to low-Mg^{2+} medium showed a higher percentage of dead neurons ($n=15$; 27.6±2.8%) when compared with cultures treated with aCSF ($n=9$; 11.9±1.8%; $P<0.001$). In addition, low-Mg^{2+}-induced neuronal cell death could be significantly reduced by adding complex I substrate pyruvate (5mM; 18.7±1.4%; $n=15$; $P<0.05$; Fig. 7C).

Neuronal death increased significantly when comparing 24 hours to 2 hours of low-Mg^{2+} exposure (42.2±3.3% vs 27.6±2.8%; $P<0.01$). Adding pyruvate to the low-Mg^{2+} medium significantly decreased neuronal death when compared with low-Mg^{2+} treatment alone ($n=15$; 27.7±1.2%; $P<0.001$; Fig. 7D).

Discussion

Using live-cell imaging, we have established a sequence of events during seizure-like activity leading to neuronal cell death in the low-Mg^{2+} seizure model. We have shown that neuronal Ca^{2+} signals in the low-Mg^{2+} model are dependent on synaptic release of glutamate acting at NMDA receptors. This Ca^{2+} signal leads to mitochondrial membrane potential depolarisation in the somata of neurons. To our knowledge, this study, for the first time, correlates Ca^{2+} signals with both mitochondrial membrane potential changes and kinetic alterations in ATP in neurons, providing strong support for the hypothesis that mitochondrial dysfunction leads to energy failure and cell death in seizures and epilepsy.

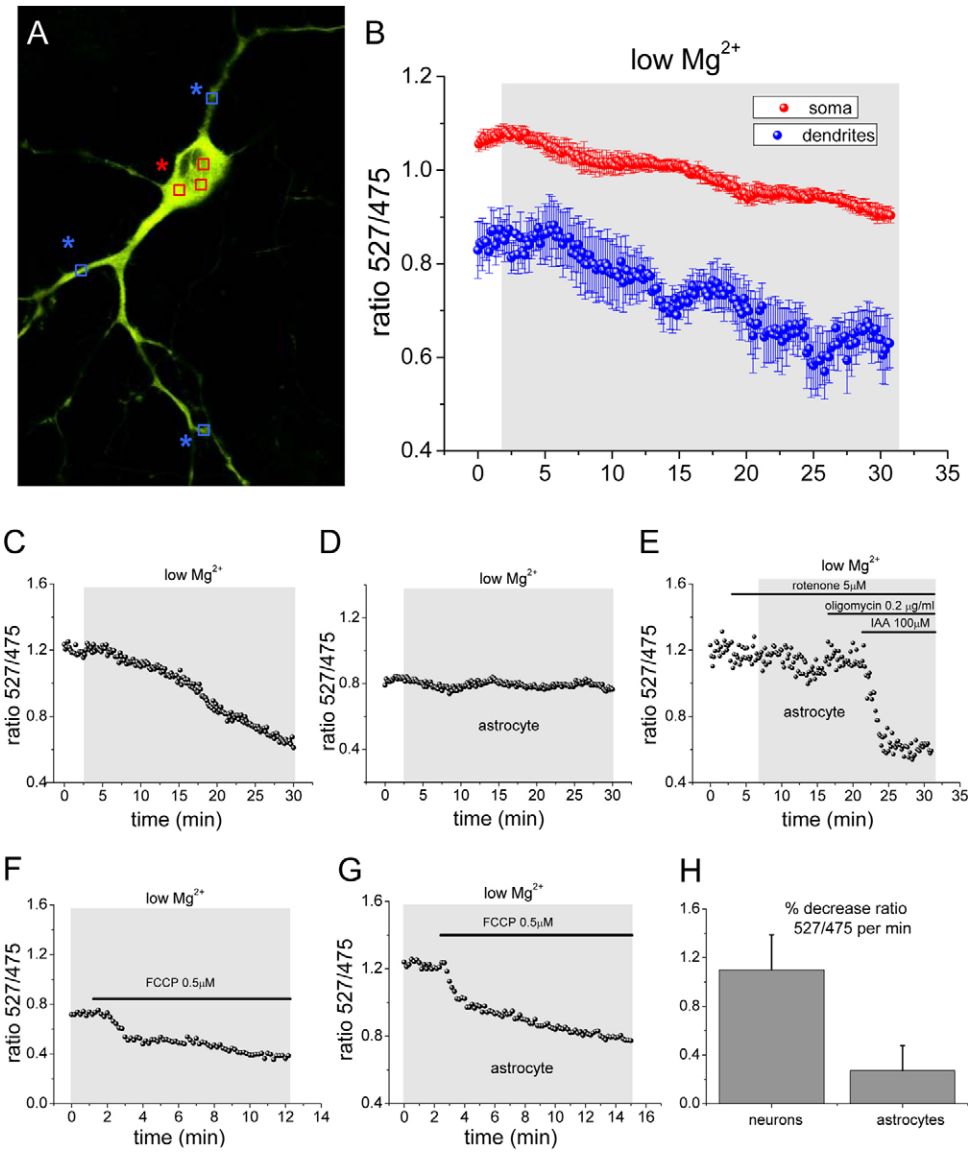

Fig. 6. Low-Mg^{2+}-induced changes in ATP as measured by genetically encoded ATP indicator AT1.03. (**A**) A neuron transfected with fluorescent indicator AT1.03. Both the neuronal soma and the dendrites showed a decrease in the ATP content after low-Mg^{2+} exposure. (**B**) Mean (±s.e.m.) ATP level measured as fluorescent ratio (527/475) decrease during low-Mg^{2+} exposure at different regions within the soma (red) and dendrites (blue) of the neuron shown in A. Note that basal ATP levels in the soma are higher when compared with dendritic ATP levels. (**C**) Ratiometrically measured ATP level in the soma of a single neuron during low-Mg^{2+} exposure. Neuronal ATP levels decreased. (**D**) ATP levels in a single astrocyte. (**E**) Astrocytic ATP levels during low-Mg^{2+} exposure are insensitive to rotenone and oligomycin exposure, but show a profound depletion after inhibition of glycolysis by iodoacetate acid (IAA). Both neuronal and astrocytic ATP depletion is accelerated with FCCP as shown by the rapid decrease of fluorescence 527/475 ratio in a single neuron (**F**) and astrocyte (**G**). (**H**) The bar chart shows the mean (±s.e.m.) neuronal compared with astrocytic ATP decrease after low Mg^{2+} exposure.

Previous studies have characterised epileptiform activity in the low-Mg^{2+} culture model of epilepsy by means of electrophysiological recordings and in part by direct Ca^{2+} measurements (DeLorenzo et al., 2005). Low-Mg^{2+}-induced Ca^{2+} oscillations were dependent on extracellular Ca^{2+} but influenced by internal Ca^{2+} stores because the SERCA inhibitor thapsigargin significantly increased the frequency of the Ca^{2+} signal. This supports a role of SERCA in impairing Ca^{2+} homeostasis in the low-Mg^{2+} culture model of epilepsy (Pal et al., 2001). Our findings of NMDA-receptor-dependent Ca^{2+} oscillations are in line with previous reports reporting NMDA receptor dependence of electrographic discharges in the low-Mg^{2+} neuronal culture model of epilepsy (DeLorenzo et al., 2005; Mangan and Kapur, 2004). The Ca^{2+} signal observed in neurons was also blocked by concanamycin A, a specific inhibitor of the vacuolar H^{+}-ATPase, indicating its dependence on vesicular release (Huss et al., 2002). Ictal, but not interictal, discharges in rat brain slices have been associated with Ca^{2+} changes in astrocytes (Gómez-Gonzalo et al., 2010), and therefore such a finding in our model lends support to this as a model of ictal rather than interictal events. We also observed similar (although lower amplitude) neuronal Ca^{2+} oscillations in another commonly used in vitro model (the 4-AP model) indicating that the observed Ca^{2+} changes are not a peculiarity of this model.

There is a close interplay between Ca^{2+} buffering at the inner mitochondrial membrane and mitochondrial depolarisation, because the Ca^{2+} electrochemical gradient favours Ca^{2+} uptake at high membrane potential (Brand, 1985; Baysal et al., 1994). Mitochondrial depolarisation has been linked to intracellular rises in Ca^{2+} during evoked synaptic activity (Bindokas et al., 1998). Low-Mg^{2+}-induced mitochondrial membrane depolarisations in soma and dendrites have been observed as transient phenomena time-locked to seizure-like events in hippocampal slice cultures (Kovács et al., 2005). However, we found that this depolarisation was sustained, and correlated with the onset of Ca^{2+} spiking, indicating a progressive decrease in the mitochondrial functional Ca^{2+}-buffering reserve. The fluctuations that were seen in dendrites are non-CsA dependent and are probably linked to the reversible Ca^{2+} fluctuations in dendrites. In our experiments,

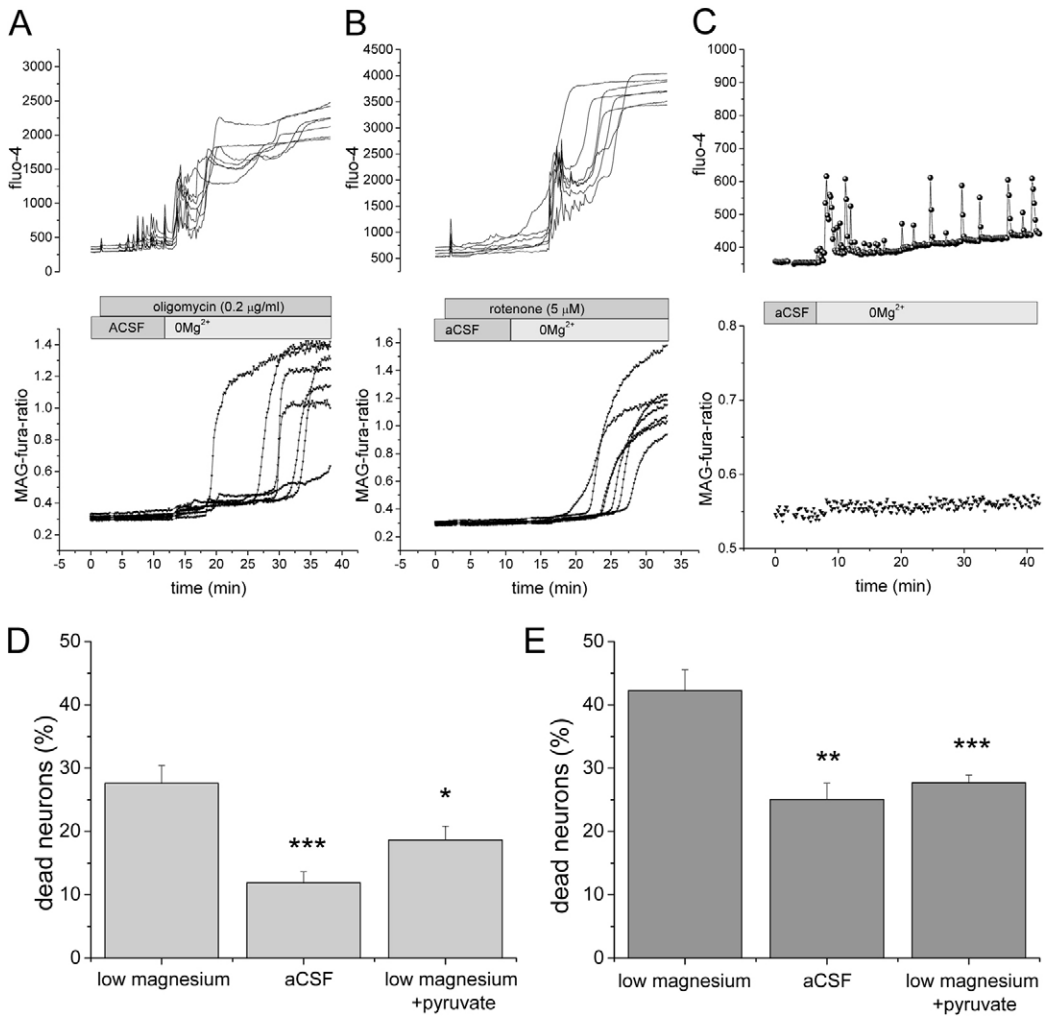

Fig. 7. ATP depletion, mitochondrial substrates and cell death. (**A**,**B**) Neuronal ATP depletion measured as an increase in MAG-Fura ratio was accelerated by blocking mitochondrial complex I with rotenone (A) or by blocking mitochondrial complex V with oligomycin (B). (**C**) Control traces without pharmacological manipulation. (**D**,**E**) The percentage of dead neurons is higher in cultures exposed to low Mg^{2+} when compared with exposure to aCSF for 2 hours (D) or 24 hours (E). Substitution of with pyruvate significantly decreased the number of dead neurons in low-Mg^{2+} conditions in both the 2 and 24 hour treatment groups. Results show mean ± s.e.m. *$P<0.05$; **$P<0.01$; ***$P<0.001$.

the cells demonstrated CsA-dependent mitochondrial depolarisation in the soma, suggesting mitochondrial permeability transition pore opening and induction of mechanisms leading to cell death (Abramov et al., 2004; Abramov and Duchen, 2008; Kovács et al., 2005).

Astrocytes are increasingly recognised as playing a pivotal role in seizures and epilepsy (Gómez-Gonzalo et al., 2010). In contrast to neurons, for the first time we found that astrocytes showed significant mitochondrial membrane potential hyperpolarisation in the low-Mg^{2+} culture model of epilepsy. Mitochondrial membrane potential changes in astrocytes can be explained by the modest Ca^{2+} signal which has been previously shown to enhance mitochondrial respiration and consequently lead to mitochondrial membrane potential hyperpolarisation (Nicholls and Budd, 2000).

We have provided evidence of a direct link of NMDA receptor Ca^{2+} spikes and mitochondrial dysfunction because inhibiting NMDA receptors or glutamate release prevented mitochondrial membrane potential depolarisation. High concentrations of glutamate and consequent binding to NMDA receptors dissipate $\Delta\psi_m$ and are sensitive to CsA (White and Reynolds, 1996), an inhibitor of MPTP opening (Zoratti and Szabò, 1995). Concordant with these findings, we found no depolarisation of mitochondrial membrane potential despite Ca^{2+} signals in CsA- and low-Mg^{2+}-treated neuronal cultures. These data provide evidence that MPTP is involved in the mitochondrial depolarisation. Our findings contrast with a previous report that found an MPTP-independent mitochondrial membrane potential depolarisation in low Mg^{2+} induced activity in hippocampal slice cultures (Kovács et al., 2005).

Real-time imaging of changes in ATP can be performed by measuring alterations in intracellular Mg^{2+}. Free $[Mg^{2+}]_c$ increases during ATP depletion through hydrolysis of MgATP (Abramov and Duchen, 2010). Increases in the MAG-Fura ratio therefore reflect intracellular ATP depletion. Seizure-induced ATP depletion has been found by analysing brain homogenates in several seizure models in vivo (Duffy et al., 1975; Gupta et al., 2000; Chapman et al., 1977; Folbergrová et al., 1981). The

amount of reduction of ATP varies in these reports, with values of 2–5% below baseline (Folbergrová et al., 1981; Chapman et al., 1977). MAG-Fura ratios in neurons showed a stepwise increase in intracellular Mg^{2+}, indicating a reduction in ATP, after omission of Mg^{2+} from the solution (Fig. 4A). This immediate transient initial increase in Mg^{2+} has been observed previously in glutamate-induced increases in intracellular free Mg^{2+}. It has been attributed to Ca^{2+} binding to intracellular sites that are usually occupied by Mg^{2+}. However, long-lasting increases in Mg^{2+} have not been observed (Brocard et al., 1993). We found that prolonged seizures lead to a depletion of ATP in neurons, but not in astrocytes, and this depletion correlated with the frequency of the oscillatory Ca^{2+} signal (Fig. 4). To provide more direct evidence of the involvement of mitochondria in this process, we incubated the cultures with FCCP. FCCP reduces mitochondrial membrane potential and therefore inhibits both Ca^{2+} uptake and ATP synthesis, and might even enhance consumption of ATP itself (Atlante et al., 2005). We found that neurons exposed to FCCP in low Mg^{2+} and in epileptiform, but not in non-epileptiform conditions, experience an energy collapse. This excessive energy depletion coincides with the first Ca^{2+} signals, suggesting that additional Ca^{2+} buffering by mitochondria further depolarises the mitochondrial membrane potential. Therefore, our findings for the first time demonstrate a tight link between ATP consumption and the time course of mitochondrial Ca^{2+}-buffering capacity exhaustion during epileptiform activity. The 'sensitising' effect of FCCP on ATP depletion can be explained by the voltage dependence of the PTP because rapid ATP depletion was delayed when inhibiting neuronal mitochondrial membrane potential depolarisation with CsA (Bernardi, 1992; Petronilli et al., 1994). Our findings strengthen the hypothesis that MPTP opening is involved in the events finally leading to neuronal ATP depletion and cell death: a finding that is also supported by in vivo models of epilepsy (Santos and Schauwecker, 2003). However, depolarisation of the mitochondrial membrane alone cannot explain the rapid ATP depletion because ATP depletion was also accelerated when inhibiting complex I with rotenone or ATP-synthetase with oligomycin. Oligomycin hyperpolarises the mitochondrial membrane, and therefore rapid ATP depletion in neurons pretreated with oligomycin can be attributed to ATP synthetase inhibition alone. In line with our findings, excessive ATP depletion in neurons has been shown in glutamate toxicity where pretreatment with FCCP leads to cell collapse (Abramov and Duchen, 2010). To confirm ATP depletion with more direct measurements and to investigate ATP changes in different cellular compartments, we conducted experiments with a genetically encoded ATP probe. Our findings provide evidence of ATP depletion in neurons during epileptiform activity as measured with the genetically encoded ATP probe. Compared with neurons that lack the glycolysis-promoting enzyme 6-phosphofructo-2-kinase/fructose 2,6-bisphosphatase, isoform 3 (PFKFB3), astrocytes exhibit a high functional reserve of this enzyme (Bolaños et al., 2010). Our data shows that ATP depletion in astrocytes during epileptiform activity can be accelerated by inhibition of glycolysis, indicating upregulation of PFKFB3.

Low-Mg^{2+}-induced cell death was described previously in hippocampal neuronal cultures (Deshpande et al., 2008). Furthermore, pyruvate substitution protects against kainate-induced epileptic brain damage in rats (Kim et al., 2010). There is evidence that in chronic epileptic tissue the monocarboxylate transporter 1, which facilitates the transport of pyruvate and other metabolic substrates across the blood–brain barrier, is deficient (Lauritzen et al., 2011). In bicuculline-induced seizures in vivo, pyruvate decreased initially and then increased, possibly pointing to a secondary compensatory mechanism (Chapman et al., 1977). We found that substitution of pyruvate protected neurons against low-Mg^{2+}-induced cell damage. Our observations whereby synaptically released glutamate mediates Ca^{2+} oscillations, mitochondrial depolarisation, and energy failure and cell death, indicate a number of steps at which interventions could be aimed to prevent neuronal death in prolonged seizures.

Materials and Methods

Cortical cell cultures

Mixed cultures of cortical neurones and glial cells from postnatal (P0) Sprague-Dawley rats were used and processed as described previously according to a modification of the protocol described by Deitch and Fischer (Haynes, 1999) (UCL breeding colony). Rat brains were quickly removed and neocortical tissue was isolated and submerged in ice-cold HBSS (Ca^{2+}, Mg^{2+}-free, Gibco-Invitrogen, Paisley, UK). The tissue was treated with 1% trypsin for 15 minutes at 37℃ to dissociate cells. After removal of residual trypsin the tissue was triturated, plated on poly-D-lysine- or laminin-coated coverslips and cultured in Neurobasal A medium (Gibco-Invitrogen) supplemented with B-27 (Gibco-Invitrogen) and 2 mM L-glutamine. Neocortical cultures were fed once a week and kept at 37℃ in a humidified atmosphere containing 5% CO_2 and 95% air. Repetitive Ca^{2+} spikes were observed in cultures from 12 days in vitro (DIV) onwards, coinciding with synapse formation. Therefore, neocortical cultures were used for experiments at 12–15 DIV. Neurons were distinguished from glia by their typical appearance using phase-contrast imaging with smooth rounded somata, bright-phase and distinct processes.

Transfection of cortical cell cultures with the genetically encoded ATP indicator AT1.03 and mitAT1.03

At day 11, cells were transfected with plasmid encoding AT1.03 DNA. The ATP probe AT1.03 has been validated extensively for real-time monitoring of ATP levels in single living cells. AT1.03 measures only free ATP, not Mg^{2+}-bound ATP and thus fluorescence of the ATP indicator represents the free available ATP pool. Ratiometric analysis of the cyan- and yellow-fluorescent proteins allows estimation of ATP kinetics within single cells (Imamura et al., 2009). We used two differentially designed probes. AT1.03 was without a targeting sequence and was expressed in neurons and astrocytes mainly in the cytoplasm, and slightly in the nucleus. MitAT1.03 specifically targeted ATP in the mitochondrial matrix by targeting the cytochrome c oxidase subunit VIII (Imamura et al., 2009). Cells were transfected with plasmid coding cDNA by using lipofectamine 2000 reagent (Invitrogen). Between 1 and 2 days after transfection, cells were subjected to imaging.

Imaging of intracellular Ca^{2+} ($[Ca^{2+}]_c$), intracellular Mg^{2+} ($[Mg^{2+}]_c$) and mitochondrial membrane potential ($\Delta\psi_m$)

Previous studies have demonstrated a tight link between electrophysiological epileptiform discharges and Ca^{2+} transients in cultures and slices (Kovács et al., 2005; Trevelyan et al., 2006). We therefore monitored oscillatory epileptiform activity with a Ca^{2+}-sensitive dye (supplement 1). Before recording, neocortical neuronal cultures were incubated for 30 minutes at room temperature with 5 μM Fura-AM, 5 μM Fura-2FF, MAG-Fura-AM or Fluo-4 AM and 0.005% pluronic in a HEPES-buffered salt solution, which is referred to as aCSF (125 mM NaCl, 2.5 mM KCl, 2 mM $MgCl_2$, 1.25 mM KH_2PO_4, 2 mM $CaCl_2$, 30 mM glucose and 25 mM HEPES, pH adjusted to 7.4 with NaOH). For simultaneous measurement of $[Ca^{2+}]_c$ and $\Delta\psi_m$, Rhodamine123 (Rh123) (10 μM) was added into the culture dishes during the last 15 minutes of the Fura-2 loading period. Cells were then washed. To correlate Mg^{2+} changes with Ca^{2+} spikes, $[Mg^{2+}]_c$ images were performed simultaneously with $[Ca^{2+}]_c$ images using MAG-Fura-AM and Fluo-4 AM. Experiments were carried out in the HEPES buffered salt solution including (aCSF) or excluding $MgCl_2$ (low Mg^{2+}). Experiments with Ca^{2+}-free medium were performed with aCSF omitting Ca^{2+} and adding a Ca^{2+} chelator (Ca^{2+} free + 0.5 mM EGTA). Fluorescence images were made on an epifluorescence inverted microscope equipped with a 20× fluorite objective. Measurements of $[Ca^{2+}]_c$ and mitochondrial membrane potential were performed in single cells using excitation light provided by a xenon arc lamp, the beam passing through a monochromator at 340, 380, and 490 nm with bandwidth of 10 nm (Cairn Research, Faversham, UK). Emitted fluorescent light was reflected through a 515 nm long-pass filter to a cooled CCD camera (Retiga; QImaging) and digitised to 12-bit resolution. Imaging data were analysed using software from Andor (Belfast, UK). Traces are presented

as the ratio of excitation at 340 and 380 nm, both with emission at >515 nm. We acquired fluorescent data with a frame interval of 10 seconds. $[Ca^{2+}]_c$ was expressed by the Fura ratio and was not calibrated because of inaccuracies arising from different calibration methods. An increase of Rhodamine123 signal indicates depolarisation of mitochondria. Rhodamine123 signals were normalised to the baseline level (set 0) and maximum signal produced by mitochondrial oxidative phosphorylation uncoupling with carbonylcyanide-p-trifluoromethoxyphenyl hydrazone (FCCP, 1 μM; set to 100). Each experiment was repeated three or more times using 2–4 different cultures.

Imaging of intracellular ATP levels with FRET-based genetically encoded indicator AT1.03

Measurements of ATP levels with AT1.03 and mitAT1.03 were performed on a confocal microscope (Zeiss 710 LSM) with an integrated META detection system. Images were obtained using a 63× oil-immersion objective to allow immediate measurement of the fluorescent signal over dendrites. Cyan fluorescent protein was excited with 405 nm, and emission from 460 to 510 nm was scanned. The 405 nm laser line was used to excite yellow fluorescent protein, which was measured using a band-pass filter from 515 to 580 nm. Illumination intensity was kept to a minimum (at 0.1–0.2% of laser output) to avoid phototoxicity and the pinhole set to give an optical slice of ~2 μm. The measurements with the ATP probe were performed in the same glucose-based medium (aCSF) that has been used for all other experimental procedures.

Drugs

All drugs were purchased from Tocris, Bristol, UK, unless indicated otherwise. D-(-)-2-amino-5-phosphonopentanoic acid (APV; 25 μM), indole-3-acetic acid sodium salt (IAA; Sigma) and Verapamil (20 μM) were dissolved in distilled water. Oligomycin (0.2 μg/ml; Sigma), rotenone (1 μM) cyclosporin A (CsA, 1 μM), concanamycin A (5 μM) and carbonylcyanide-p-trifluoromethoxyphenyl hydrazone (FCCP; 0.5 or 1 μM) were dissolved in dimethyl sulfoxide (DMSO). All drugs were stored as 1000 times stocks at −20℃. Drugs were dissolved in aCSF to achieve their final concentrations during experiments.

Cell-viability experiment

To asses cell death, cells were stained simultaneously with 20 μM propidium iodide, which is excluded from viable cells but exhibits a red fluorescence in nonviable cells following a loss of membrane integrity, and 4.5 μM Hoechst 33342 (Molecular Probes, Eugene, OR), which labels nuclei blue, to count the total number of cells. Each experiment was repeated on at least 3–4 different coverslips from independent cultures. Three to four representative regions per coverslip were photographed and analysed. Statistical analysis was performed on the regions.

Statistical analyses

Statistical analyses (two-tailed Student's *t*-test, one sample *t*-test, one-way ANOVA and Pearson's correlation) were performed using SPSS 17.0 (Chicago, IL). The significance level was set at $P<0.05$ and all data are given as mean ± s.e.m. Analyses were performed on single cells (Ca^{2+}, Mg^{2+} and $\Delta\psi_m$ measurements) or regions (cell-death analysis). In simultaneous recordings, the analysis was performed on the same cells to allow for correlation analysis of double-stained cells.

Acknowledgements

The constructs for the measurements of ATP were generously provided by Hiromi Imamura, The Hakubi Center & Graduate School of Biostudies, Kyoto University.

Funding

S.K. was supported by a stipend from the Deutsche Forschungsgemeinschaft [grant number KO-3878/1-1].

References

Abramov, A. Y. and Duchen, M. R. (2008). Mechanisms underlying the loss of mitochondrial membrane potential in glutamate excitotoxicity. *Biochim. Biophys. Acta* **1777**, 953-964.

Abramov, A. Y. and Duchen, M. R. (2010). Impaired mitochondrial bioenergetics determines glutamate-induced delayed calcium deregulation in neurons. *Biochim. Biophys. Acta* **1800**, 297-304.

Abramov, A. Y., Canevari, L. and Duchen, M. R. (2004). Calcium signals induced by amyloid beta peptide and their consequences in neurons and astrocytes in culture. *Biochim. Biophys. Acta* **1742**, 81-87.

Ascher, P., Bregestovski, P. and Nowak, L. (1988). N-methyl-D-aspartate-activated channels of mouse central neurones in Mg^{2+}-free solutions. *J. Physiol.* **399**, 207-226.

Atlante, A., Giannattasio, S., Bobba, A., Gagliardi, S., Petragallo, V., Calissano, P., Marra, E. and Passarella, S. (2005). An increase in the ATP levels occurs in cerebellar granule cells en route to apoptosis in which ATP derives from both oxidative phosphorylation and anaerobic glycolysis. *Biochim. Biophys. Acta* **1708**, 50-62.

Baysal, K., Jung, D. W., Gunter, K. K., Gunter, T. E. and Brierley, G. P. (1994). Na(+)-dependent Ca^{2+} efflux mechanism of heart mitochondria is not a passive Ca^{2+}/2Na+ exchanger. *Am. J. Physiol.* **266**, C800-C808.

Bernardi, P. (1992). Modulation of the mitochondrial cyclosporin A-sensitive permeability transition pore by the proton electrochemical gradient. Evidence that the pore can be opened by membrane depolarization. *J. Biol. Chem.* **267**, 8834-8839.

Bindokas, V. P., Lee, C. C., Colmers, W. F. and Miller, R. J. (1998). Changes in mitochondrial function resulting from synaptic activity in the rat hippocampal slice. *J. Neurosci.* **18**, 4570-4587.

Bolaños, J. P., Almeida, A. and Moncada, S. (2010). Glycolysis: a bioenergetic or a survival pathway? *Trends Biochem. Sci.* **35**, 145-149.

Brand, M. D. (1985). The stoichiometry of the exchange catalysed by the mitochondrial calcium/sodium antiporter. *Biochem. J.* **229**, 161-166.

Brocard, J. B., Rajdev, S. and Reynolds, I. J. (1993). Glutamate-induced increases in intracellular free Mg^{2+} in cultured cortical neurons. *Neuron* **11**, 751-757.

Castilla-Guerra, L., del Carmen Fernández-Moreno, M., López-Chozas, J. M. and Fernández-Bolaños, R. (2006). Electrolytes disturbances and seizures. *Epilepsia* **47**, 1990-1998.

Chapman, A. G., Meldrum, B. S. and Siesjö, B. K. (1977). Cerebral metabolic changes during prolonged epileptic seizures in rats. *J. Neurochem.* **28**, 1025-1035.

Corkey, B. E., Duszynski, J., Rich, T. L., Matschinsky, B. and Williamson, J. R. (1986). Regulation of free and bound Mg^{2+} in rat hepatocytes and isolated mitochondria. *J. Biol. Chem.* **261**, 2567-2574.

Damiano, M., Galvan, L., Déglon, N. and Brouillet, E. (2010). Mitochondria in Huntington's disease. *Biochim. Biophys. Acta* **1802**, 52-61.

DeLorenzo, R. J., Sun, D. A. and Deshpande, L. S. (2005). Cellular mechanisms underlying acquired epilepsy: the calcium hypothesis of the induction and maintainance of epilepsy. *Pharmacol. Ther.* **105**, 229-266.

Deshpande, L. S., Lou, J. K., Mian, A., Blair, R. E., Sombati, S., Attkisson, E. and DeLorenzo, R. J. (2008). Time course and mechanism of hippocampal neuronal death in an in vitro model of status epilepticus: role of NMDA receptor activation and NMDA dependent calcium entry. *Eur. J. Pharmacol.* **583**, 73-83.

Distelmaier, F., Koopman, W. J., van den Heuvel, L. P., Rodenburg, R. J., Mayatepek, E., Willems, P. H. and Smeitink, J. A. (2009). Mitochondrial complex I deficiency: from organelle dysfunction to clinical disease. *Brain* **132**, 833-842.

Duffy, T. E., Howse, D. C. and Plum, F. (1975). Cerebral energy metabolism during experimental status epilepticus. *J. Neurochem.* **24**, 925-934.

Folbergrová, J., Ingvar, M. and Siesjö, B. K. (1981). Metabolic changes in cerebral cortex, hippocampus, and cerebellum during sustained bicuculline-induced seizures. *J. Neurochem.* **37**, 1228-1238.

Gómez-Gonzalo, M., Losi, G., Chiavegato, A., Zonta, M., Cammarota, M., Brondi, M., Vetri, F., Uva, L., Pozzan, T., de Curtis, M. et al. (2010). An excitatory loop with astrocytes contributes to drive neurons to seizure threshold. *PLoS Biol.* **8**, e1000352.

Gupta, R. C., Milatovic, D., Zivin, M. and Dettbarn, W. D. (2000). Seizure-induced changes in energy metabolites and effects of N-tert-butyl-alpha-phenylnitrone (PNB) and vitamin E in rats. *Pflügers Arch.* **440**, R160-R162.

Haynes, L. W. (ed.) (1999). *The Neuron In Tissue Culture*. Chichester: Wiley.

Huss, M., Ingenhorst, G., König, S., Gassel, M., Dröse, S., Zeeck, A., Altendorf, K. and Wieczorek, H. (2002). Concanamycin A, the specific inhibitor of V-ATPases, binds to the V(o) subunit c. *J. Biol. Chem.* **277**, 40544-40548.

Imamura, H., Nhat, K. P., Togawa, H., Saito, K., Iino, R., Kato-Yamada, Y., Nagai, T. and Noji, H. (2009). Visualization of ATP levels inside single living cells with fluorescence resonance energy transfer-based genetically encoded indicators. *Proc. Natl. Acad. Sci. USA* **106**, 15651-15656.

Kim, J.-E., Ryu, H. J., Kim, M.-J., Kim, D.-W., Kwon, O.-S., Choi, S. Y. and Kang, T.-C. (2010). Pyridoxal-5′-phosphate phosphatase/chronophin induces astroglial apoptosis via actin-depolymerizing factor/cofilin system in the rat brain following status epilepticus. *Glia* **58**, 1937-1948.

Kim, T.-Y., Yi, J.-S., Chung, S.-J., Kim, D.-K., Byun, H.-R., Lee, J.-Y. and Koh, J.-Y. (2007). Pyruvate protects against kainate-induced epileptic brain damage in rats. *Exp. Neurol.* **208**, 159-167.

Kovács, R., Kardos, J., Heinemann, U. and Kann, O. (2005). Mitochondrial calcium ion and membrane potential transients follow the pattern of epileptiform discharges in hippocampal slice cultures. *J. Neurosci.* **25**, 4260-4269.

Lauritzen, F., de Lanerolle, N. C., Lee, T.-S., Spencer, D. D., Kim, J. H., Bergersen, L. H. and Eid, T. (2011). Monocarboxylate transporter 1 is deficient on microvessels in the human epileptogenic hippocampus. *Neurobiol. Dis.* **41**, 577-584.

Mangan, P. S. and Kapur, J. (2004). Factors underlying bursting behavior in a network of cultured hippocampal neurons exposed to zero Mg^{2+}. *J. Neurophysiol.* **91**, 946-957.

Mitchell, P. and Moyle, J. (1965). Evidence discriminating between the chemical and the chemiosmotic mechanisms of electron transport phosphorylation. *Nature* **208**, 1205-1206.

Nicholls, D. G. and Budd, S. L. (2000). Mitochondria and neuronal survival. *Physiol. Rev.* **80**, 315-360.

Pal, S., Sun, D., Limbrick, D., Rafiq, A. and DeLorenzo, R. J. (2001). Epileptogenesis induces long-term alterations in intracellular calcium release and sequestration mechanisms in the hippocampal neuronal culture model of epilepsy. *Cell Calcium* **30**, 285-296.

Petronilli, V., Costantini, P., Scorrano, L., Colonna, R., Passamonti, S. and Bernardi, P. (1994). The voltage sensor of the mitochondrial permeability transition pore is tuned by the oxidation-reduction state of vicinal thiols. Increase of the gating potential by oxidants and its reversal by reducing agents. *J. Biol. Chem.* **269**, 16638-16642.

Pitkänen, A., Nissinen, J., Nairismägi, J., Lukasiuk, K., Gröhn, O. H., Miettinen, R. and Kauppinen, R. (2002). Progression of neuronal damage after status epilepticus and during spontaneous seizures in a rat model of temporal lobe epilepsy. *Prog. Brain Res.* **135**, 67-83.

Rusakov, D. A. and Fine, A. (2003). Extracellular Ca^{2+} depletion contributes to fast activity-dependent modulation of synaptic transmission in the brain. *Neuron* **37**, 287-297.

Santos, J. B. and Schauwecker, P. E. (2003). Protection provided by cyclosporin A against excitotoxic neuronal death is genotype dependent. *Epilepsia* **44**, 995-1002.

Swanson, T. H. (1995). The pathophysiology of human mesial temporal lobe epilepsy. *J. Clin. Neurophysiol.* **12**, 2-22.

Trevelyan, A. J., Sussillo, D., Watson, B. O. and Yuste, R. (2006). Modular propagation of epileptiform activity: evidence for an inhibitory veto in neocortex. *J. Neurosci.* **26**, 12447-12455.

Wasterlain, C. G., Fujikawa, D. G., Penix, L. and Sankar, R. (1993). Pathophysiological mechanisms of brain damage from status epilepticus. *Epilepsia* **34**, S37-S53.

White, R. J. and Reynolds, I. J. (1996). Mitochondrial depolarization in glutamate-stimulated neurons: an early signal specific to excitotoxin exposure. *J. Neurosci.* **16**, 5688-5697.

Yi, J.-S., Kim, T.-Y., Kyu Kim, D. and Koh, J.-Y. (2007). Systemic pyruvate administration markedly reduces infarcts and motor deficits in rat models of transient and permanent focal cerebral ischemia. *Neurobiol. Dis.* **26**, 94-104.

Zoratti, M. and Szabò, I. (1995). The mitochondrial permeability transition. *Biochim. Biophys. Acta* **1241**, 139-176.